ISSN 1330-3651 (Print), ISSN 1848-6339 (Online) https://doi.org/10.17559/TV-20230703000782
Original scientific paper

# Optimal Disturbance Control for Energy Feedback of Gas Water Heaters

Qian WANG*, Wei LI, Xue-qin MENG, Chun-lan LI

**Abstract:** In order to improve the recovery and utilization of hot water energy in gas water heater pipes, a self-powered solution is proposed in this study. The proposed solution focuses on improving energy collection efficiency by increasing the heat transfer coefficient of the water flow and tracking the maximum output power of the temperature plate. The design of heat transfer structure, power characteristics of temperature plate and circuit conversion are analyzed. In order to verify the feasibility of the proposed solution, a test device was constructed for physical testing and verification. The experimental results demonstrate the successful implementation of the self-powered gas water heater. The special structure and perturbation method used enable the experimental device to achieve the maximum power output, and the experimental device can continuously provide 300mW output power. This research contributes to the development of energy -efficient and self-powered gas water heater solutions, offering potential benefits for energy saving and sustainable use in the residential sector.

**Keywords:** disturbance; energy harvesting; heat transfer coefficient; maximum power; self-powered

## 1 INTRODUCTION

Energy collection is a way to use energy efficiently, generally by converting weak energy into electrical energy output or storage [1-5]. It is widely used in low-power intermittent working scenarios. Common methods include light energy collection, sound energy collection, thermal energy collection, vibration energy collection, etc. [6]. Energy collection is mainly a process of converting and storing residual energy. With the development of sensor technology in recent years, the application of heat energy collection has been widely used [7]. The conversion of thermal energy into electricity, from the first discovery of the thermoelectric effect by French physicist Partier in 1834 [8], has developed for nearly 200 years, and the most common conversion method uses thermoelectric sheets. Thermoelectric sheets, also called temperature platesheets [9], use the thermoelectric effect to achieve electrical energy output. They have advantages of simple structure, small size, light weight, and no pollution. The output power is directly related to the temperature difference between the hot and cold ends of the thermometer. The greater the temperature difference, the higher the output power. Hence in practical applications, the energy conversion efficiency is low, and improving the conversion efficiency is the future development trend of thermoelectric conversion.

## 2 LITERATURE REVIEW

In the field of thermoelectric research, in recent years, there are many interdisciplinary and cross-field scientists at home and abroad to carry out a lot of research and application of thermoelectric conversion. Zakariya M. Dalala et al. used the maximum power point tracking algorithm to measure the open circuit voltage and short circuit current of the temperature plate [10]. Nistor Daniel Trip et al. studied the matching relationship between the output resistance of the temperature plate and the power input and proposed a simulation model [11]. Hu Shenhua et al. tested the efficiency improvement of temperature difference power generation based on the algorithm of maximum power point tracking [12]. Liu Dan et al. studied the application of Ag2Se nanorods flexible thermoelectric films in temperature difference power generation [13]. Zhang Yongchang et al. used genetic algorithm to construct the module layout of high-efficiency energy conversion [14, 15]. Wu Zhidong et al. designed a pipeline temperature difference energy conversion device [16, 17], which adopts the direct tube convective disturbance method to realize the collection and utilization of hot gas energy, which is characterized by low heat transfer efficiency and can realize energy conversion within a large temperature difference range. Katche et al. designed a method of water energy collection by changing the relative position of the contact surface [18, 19], which improved the heat transfer efficiency, but the system structure was complex and its own power consumption was high. Zheng Shang et al. proposed a method of oil flow energy collection that is auxiliary to elastic potential energy [20], which requires constant supply of elastic potential energy in specific scenarios.

Liang Weiguang proposed an artificial neural network method to predict and modify the coefficient of the standard turbulence model in RANS [21], and obtained the velocity field distribution of the pipeline flow after disturbance, which could improve the accuracy of the velocity field, but this method did not consider the influence of temperature change. Zheng Haibo et al. adopted plasma flow control technology to actively control the generated turbulent boundary layer [22]. This method can achieve effective control of turbulence, but it is only applicable to fast fluid disturbance, and the effect of slow fluid disturbance is not good. Wu Yiyi proposed a method to increase the average Nusselt number to improve the convective heat transfer capacity [23], which required that the Reynolds number should be large enough, but the Reynolds number of hot and cold water could not reach the required value of the method. These studies have done a lot of demonstration and design from the theoretical model, material properties, structural design, practical engineering applications and so on. However, the implementation scheme is completed under established conditions, and the structure is complex, which is not practical and adaptable.

In this paper, a method to improve the disturbance is proposed, using pipeline structure design to enhance the turbulent velocity and heat transfer coefficient, so as to enhance the heat transfer and the energy conversion efficiency and realize the self-power supply of the gas water heater.

## 3 RESEARCH METHODS OF ENERGY HARVESTING FOR HOT AND COLD WATER

The working principle of the hot and cold water energy collection system is shown in Fig. 1. It includes four parts: heat energy absorbing mechanism, cold energy absorbing mechanism, electric energy storage mechanism and electric energy releasing mechanism.

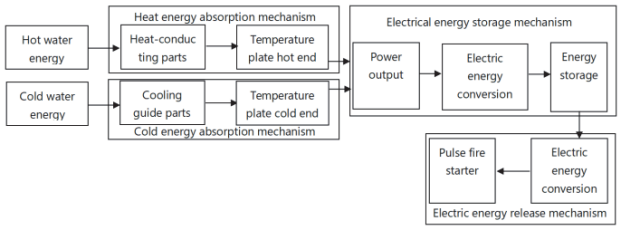


**Figure 1** System composition

The temperature difference brought by hot and cold water temperature plate is obtained and converted into voltage output. The output voltage charges the energy storage element through the booster circuit. When the gas water heater needs to work, the energy storage element releases the stored electric energy to the pulse type fire starter. In practical application, when the device is used for the first time, the energy storage element has not stored electricity, so a backup power supply (button battery) is added to the design to solve this problem.

As can be seen from the heat transfer properties, there are three measures to enhance heat transfer: increase the contact area, increase the heat transfer temperature difference, and increase the heat transfer coefficient [24, 25]. The heat energy absorption mechanism enhances heat transfer from the above three points combined with practical application characteristics. Fig. 2 shows the schematic diagram of the heat transfer mechanism on the wall of the heat energy absorbing pipe. The pipe is designed into a right-angle structure. The temperature plate is placed between the hot and cold water pipes, in the area after turning the right angle.

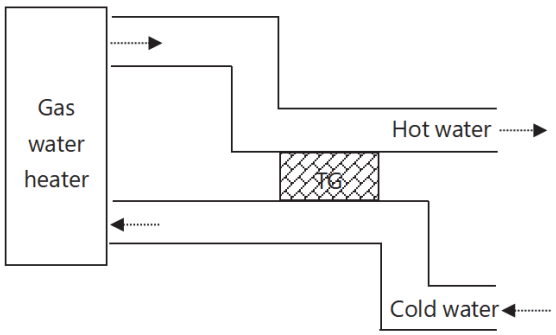


**Figure 2** Schematic diagram of heat and cold energy extraction mechanism

In order to increase the heat transfer area, square pipes with a cross-sectional area of 40 × 20 mm are adopted for the hot and cold water pipes in the heat transfer area, so as to maximize the contact between the hot and cold surfaces of the temperature difference sheet and the pipe wall. Meanwhile, thermal conductive silicon grease is applied to improve heat transfer efficiency. The hot water pipe and cold water pipe layout have a countercurrent structure, and this helps increase the heat transfer temperature difference and improve heat transfer efficiency. According to the fluid properties, when tap water flows through a square pipe, its Reynolds number can be calculated to obtain:

$$R_e = 2.64 \times 10^4 > 4000$$

The fluid flow state is in the zone of fully developed turbulence. In this case, the velocity is fastest in the turbulent core region (partial circumferential region near the center of the inner diameter section of the water pipe), decreases gradually in the transition region, and is slowest in the laminar flow. This feature reduces the heat transfer ability of the fluid to the wall of the pipe, so the pipe is designed into a right-angle shape. Under the action of the angle, the flow velocity and turbulent layer degree near the water pipe of the temperature difference sheet are improved (turbulence destroys the laminar flow), and the heat transfer coefficient of the pipe wall is increased, thereby improving the heat energy transfer.

The initial conditions are set as follows: water inlet velocity of 1 m/s, aluminum alloy wall material, and the $k$-$\varepsilon$ model (k-epsilon (2eqn)). The ANSYS simulation velocity cloud diagram of the square pipe rectangular structure is shown in Fig. 3.

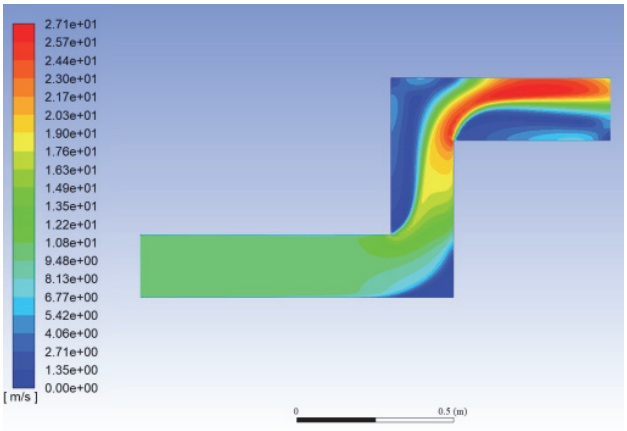


**Figure 3** Cloud chart of water velocity in a right-angled square pipe

As can be seen from the cloud diagram in Fig. 3, in the rectangular tube, the water velocity on the outer side increases significantly after the flow passes through the second right angle in the forward direction (the red area in Fig. 3), and the bottom layer of laminar flow near the tube wall basically disappears, which is conducive to improving heat transfer.

The influence of the flow velocity of the hot water flowing out of the gas water heater on the heat transfer coefficient was analyzed. The average logarithmic temperature difference range of the hot and cold water pipes was set at 18.75 ℃ to 22.64 ℃, and the temperature rise of the cold water pipes was set at 2.72 ℃. The scatter diagram and fitting curve of the influence of velocity on heat transfer coefficient are shown in Fig. 4. The fitting degree = 0.87, the fitting is good, and the fitting function is as follows:

$$k = 79.79 + 80.66 \ln(v) \quad (1)$$

Taking the derivative of Eq. (1), we can get:

$$\frac{\mathrm{d}(k)}{\mathrm{d}(v)}=\frac{80.66}{v}>0$$

That is, with the increase of velocity $v$, the heat transfer coefficient increases gradually.

$$\frac{\mathrm{d}^2(k)}{\mathrm{d}(v^2)}=\left(-\frac{80.66}{v^2}\right)<0$$

It indicates that the upward trend of heat transfer coefficient decreases with the increase of velocity $v$.

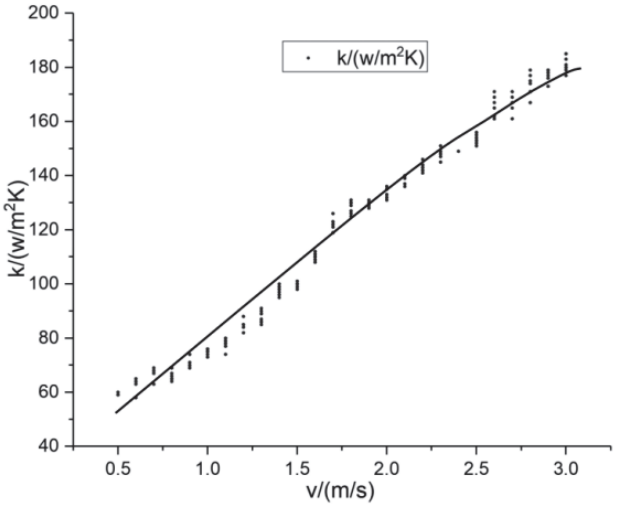


**Figure 4** *k-v* scatter plot and fitting curve

The above analysis shows that an appropriate increase in flow velocity can improve the heat transfer coefficient and thus increase the heat transfer.

The influence of the temperature difference between hot and cold water in the gas water heater on the heat transfer coefficient is analyzed. The flow rate of hot water in the water pipe is set at 1.2 m/s, and the device is tested experimentally. The scatter diagram and fitting curve of the influence of temperature difference on the heat transfer coefficient are shown in Fig. 5. The degree of fit is 0.90, and the fitting function is as follows:

$$k=99.864+0.747\Delta T-0.007\Delta T^2 \qquad (2)$$

The derivative of Eq. (2) is obtained when the temperature difference $\Delta T$ is within the range of 0 to 50 °C.

$$\frac{\mathrm{d}(k)}{\mathrm{d}(\Delta T)}=(0.747-0.014\Delta T)>0\,.$$

with the increase of temperature difference, the heat transfer coefficient $K$ gradually increases.

$$\frac{\mathrm{d}^2(k)}{\mathrm{d}(\Delta T^2)}=-0.014<0\,,$$

indicating that the increase of temperature difference $\Delta T$ and heat transfer coefficient $K$ gradually decrease.

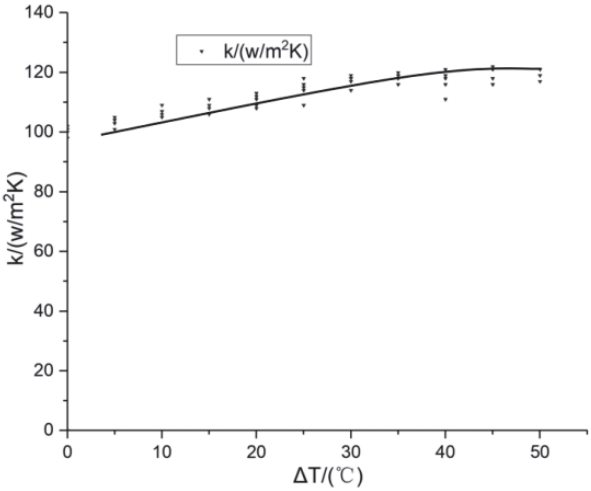


**Figure 5** *k*-Δ*T* scatter plot and fitting curve

The above analysis shows that increasing temperature difference can improve heat transfer coefficient and thus increase heat transfer.

When the temperature difference is 20 °C, 30 °C, 40 °C and 50 °C respectively, the output power changes under different loads are shown in Fig. 6. As can be seen from Fig. 6, under different temperature, the output power reaches its maximum when the load is close to 2 Ω. The maximum output power is 3.42 W at 50 ℃ temperature difference.

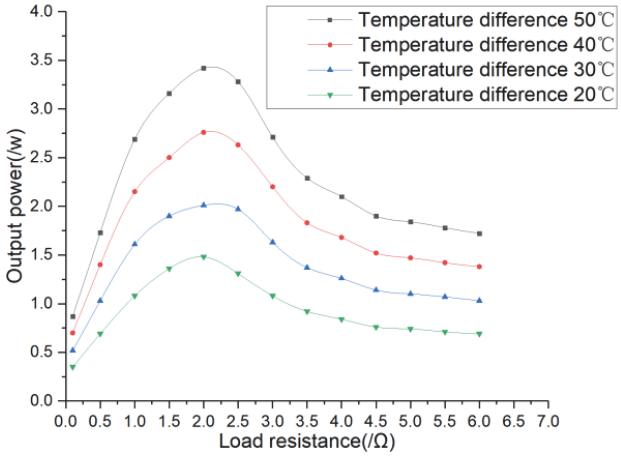


**Figure 6** Different load power curves

When the load is close to 2 Ω, the load will obtain the maximum power output by the temperature plate.

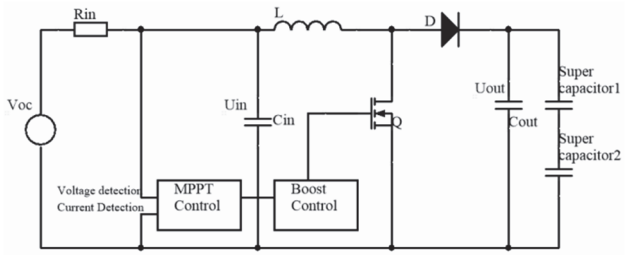


**Figure 7** Topological structure diagram of electric energy collection

The output electrical energy and storage topology of the thermograph is shown in Fig. 7. It consists of two parts: DC-DC transformation and MPPT.

The thermostatic sheet is equivalent to a voltage source ($V_{oc}$) and internal resistance ($R_{in}$) in series, and its output electric energy is charged to the energy storage unit (ultracapacitor) through the BOOST circuit. $C_{in}$, $L$, $Q$, $D$ and $C_{out}$ constitute the DC-DC conversion circuit. BOOST transform circuit is:

$$U_{out} = \frac{U_{in}}{1-D} \tag{3}$$

where, $D$ is the duty ratio of PWM wave, $U_{in}$ is the open-circuit output voltage of the temperature plate, $U_{out}$ is the BOOST output voltage.

Assuming that the conversion efficiency of DC-DC is 100% and the initial voltage of the supercapacitor is 0, the following can be obtained from energy conservation:

$$\frac{U_{in}^{\ 2}}{R_{in}}(t_{end}-0) = \frac{1}{2}C[U_C(t_{end})^2] \tag{4}$$

Get:

$$R_{in} = \frac{2(1-D)^2 t_{end}}{C} \tag{5}$$

where, $D$ is the PWM wave duty ratio, $C$ is the total capacity of the supercapacitor, and $t_{end}$ is the charging time of the supercapacitor.

By controlling duty ratio $D$, impedance matching between $R_{in}$ and energy storage capacitor can be realized to achieve maximum power output.

The MPPT controller adopts the disturbance algorithm to realize the maximum power point tracking [26-28], and realizes the maximum power point matching by adjusting the duty ratio of PWM wave of the control signal of the BOOST transform circuit.

The principle is to make a disturbance on the voltage $U_{(t-1)}$ at time $t-1$, the disturbance value is $\Delta U$, take $U_{(t-1)}+\Delta U$ as the voltage at time $t$, at the same time measure the current $I_{(t)}$ at time $t$, calculate the power value $P_{(t)}$ at time $t$, compare the power of $P_{(t)}$ and $P_{(t-1)}$, power increase, the disturbance is correct, the next step continues to disturb along the direction; when the power is reduced the disturbance is opposite, the next step is in the opposite direction. If the voltage at time $t$ is increased but the power is reduced relative to time $t-1$, the duty ratio needs to be reduced. If the voltage at time $t$ is increased relative to time $t-1$ but the power is also increased, you need to increase the duty ratio. By the power value corresponding to the PWM wave output of different duty ratios, control BOOST transform, in order to achieve the load and the output power of the temperature plate matching, to achieve the maximum power point tracking.

The perturbation steps are as follows [29]:

(1) Apply forward disturbance voltage $\Delta U_+$, $P_{(t)} > P_{(t-1)}$, and disturbance along the original direction;

(2) Apply the forward disturbance voltage $\Delta U_+$, $P_{(t)} < P_{(t-1)}$, along the opposite direction;

(3) Apply negative disturbance voltage $\Delta U_-$, $P_{(t)} > P_{(t-1)}$, disturbance along the original direction;

(4) Apply negative perturbation voltage $\Delta U_+$, $P_{(t)} < P_{(t-1)}$, and perturbation along the opposite direction;

You can find the maximum power point by following the preceding four steps.

The rated power of the electronic fire starter of the gas water heater is 300 mW and the rated voltage is 3 V. The voltage of the full terminal of the ultracapacitor will be greater than 3 V, and the voltage of the discharge terminal of the ultracapacitor will be less than 3 V. In order to make the electronic igniter work normally, the DC-DC transformation is added to realize the rated operation of the ignitor.

The power supply topology of the energy storage unit releasing electric energy to the electronic emitter is shown in Fig. 8. The topology adopts BUCK-BOOST structure with up and down pressure [30], RL as electronic flame, Rf1 and Rf2 as output sampling feedback resistors. The feedback resistor samples the output voltage and partial voltage and transmits it to the controller to control the PWM wave duty ratio ($D$), realizing the output voltage regulation process.

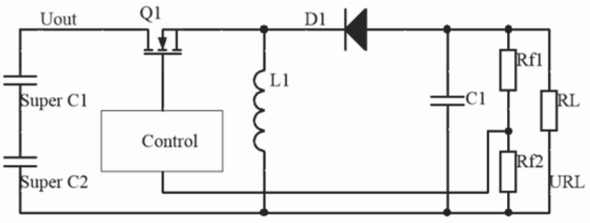


**Figure 8** Topological structure diagram of electric energy release

BUCK-BOOST conversion circuits are:

$$U_{RL} = \frac{D}{1-D}U_{Uout} \tag{6}$$

where, $D$ is the duty ratio of PWM wave.

In the physical test and production, in order to reduce the actual circuit loss, the ADP5090 power collection integrated chip is selected to store the output power of the thermograph into the ultracapacitor group. ADP5090 chip integrates BOOST module and MPPT module, starting voltage 380 mV, minimum input effective voltage 80 mV after starting, maximum input voltage 3.3 V. The energy storage device is composed of two 4.0 F/2.7 V supercapacitors in series.

The circuit is shown in Fig. 9. The reverse breakdown voltage of the regulator D1 is 3.2 V to prevent the input voltage from exceeding 3.3 V and protect the ADP5090 chip.

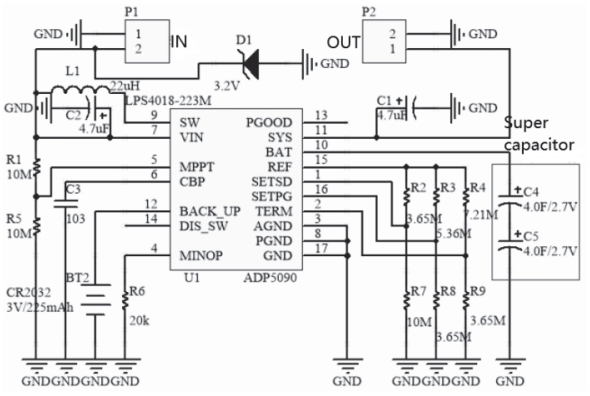


**Figure 9** Energy harvesting circuit

The supercapacitor overcharge protection threshold voltage is 5.40 V, which can be calculated as follows:

$$V_{\mathrm{TE}} = \frac{3}{2} V_{\mathrm{REF}} \times (1 + \frac{R_4}{R_9}) = \frac{3}{2} \times 1.21 \times (1 + \frac{7.21M}{3.65M}) = 5.40\mathrm{V} \quad (7)$$

The minimum discharge voltage of the supercapacitor is 1.65 V, which can be calculated as follows:

$$V_{\mathrm{SD}} = V_{\mathrm{REF}} \times (1 + \frac{R_2}{R_7}) = 1.21 \times (1 + \frac{3.65M}{10M}) = 1.65\mathrm{V} \quad (8)$$

BT2 is a lithium ion button battery CR2032, which is used as a backup battery with a nominal value of 3.0 V/225 mAh. When the output voltage of the ultracapacitor group is less than 3.0 V, the battery supplies power to the load. When the voltage of the ultracapacitor is greater than the BT2 voltage, the ultracapacitor discharges. In this way, the electronic ignition of water heater can be normally opened when the device is used for the first time.

The design uses TPS63802 chip, the chip input voltage range: 1.3 V-5.5 V; the output voltage ranges from 1.8 V to 5.2 V. The circuit is shown in Fig. 10. AGND is used in the design of PCB hole in layer after connecting to GND.

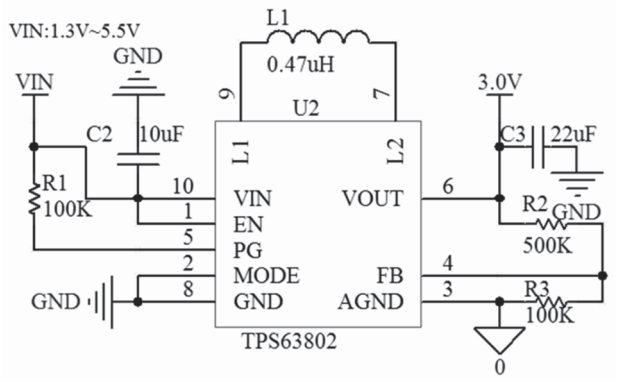


**Figure 10** 3 V voltage regulator circuit

The feedback resistance is determined by the output voltage. In the design, the output voltage is a constant 3.0 V, and the resistance values of the feedback resistors are set as R2 = 500 KΩ and R3 = 100 KΩ respectively, which just meets the conditions. The calculation is as follows:

$$V_{\mathrm{OUT}} = V_{\mathrm{REF}} \times \left(1 + \frac{R_2}{R_3}\right) = 0.5 \times \left(1 + \frac{500\mathrm{K}}{100\mathrm{K}}\right) = 3.0\mathrm{V} \quad (9)$$

Temperature plate to achieve heat energy conversion into current output; BOOST will input a small DC voltage boost to continuously charge the supercapacitor. After the water heater starts to use (during the use stage and at the end of the use), the temperature difference sheet converts the heat energy of the pipeline into electric energy and stores it in the supercapacitor through the BOOST circuit. When the gas water heater is used next time, the electric spark of the water heater can be driven by the discharge of the supercapacitor to ignite the water heater to work normally. When the gas water heater works, it can continue to make use of the temperature difference between the hot water pipe and the cold water pipe to output electric energy through the temperature difference sheet and store it in the ultracapacitor group, realizing the self-powered cycle process.

## 4 RESULTS AND DISCUSSION

Energy absorption structure uses comparative method to verify the performance of the device structure in improving heat transfer capacity. The heat transfer efficiency of the pipe with the structure shown in Fig. 2 and the straight pipe structure is compared in the test. Under the conditions of the same inlet speed (1.5 m/s), the same contact area and different temperature differences, the test data are shown in Tab. 1 below.

**Table 1** Comparison of the influence of temperature difference on the output power of the energy extraction structure

| | Right Angle pipe | | Straight pipe | |
|---|---|---|---|---|
| Temperature difference / ℃ | Output voltage / V | Output power / w | Output voltage / V | Output power / w |
| 49.9 | 4.14 | 3.89 | 3.61 | 3.42 |
| 40.7 | 3.38 | 2.76 | 2.88 | 2.44 |
| 30.5 | 2.44 | 2.12 | 2.01 | 1.87 |
| 20.8 | 1.57 | 1.36 | 1.23 | 1.25 |
| 10.3 | 0.68 | 0.23 | 0.47 | 0.24 |

As can be seen from Tab. 1, when the temperature difference is high, the output power of right-angle pipe structure increases by 13.7% compared with that of straight pipe structure, and the power difference decreases with the decrease of temperature difference. When the temperature difference is low, there is little difference between the output power of right-angle pipe and that of straight pipe.

The contact area is constant, the temperature difference is the same (50 ℃), and the flow rate is different. The test data are shown in Tab. 2 below.

**Table 2** Comparison of the influence of flow rate on the output power of the energy extraction structure

| | Right Angle pipe | | Straight pipe | |
|---|---|---|---|---|
| Velocity of flow / m/s | Output voltage / V | Output power / w | Output voltage / V | Output power / w |
| 0.5 | 3.63 | 3.76 | 3.02 | 3.39 |
| 1.0 | 3.98 | 3.81 | 3.28 | 3.41 |
| 1.5 | 4.14 | 3.88 | 3.61 | 3.42 |
| 2.0 | 4.37 | 3.96 | 3.78 | 3.48 |
| 2.5 | 4.56 | 4.04 | 3.92 | 3.53 |

As can be seen from Tab. 2, under the same flow velocity, the heat transfer of right-angle pipe is higher than that of straight pipe, and the faster the flow velocity, the heat transfer will be improved to some extent. When the flow rate increases from 0.5 m/s to 2.5 m/s, the output power increases.

The results in Tab. 1 and Tab. 2 show that the designed energy absorption results can improve the heat transfer efficiency of the temperature plate and alleviate the problem of low power generation efficiency of the temperature plate.

Tab. 1 The temperature difference increases sharply from 20 ℃ to 50 ℃. The output current, voltage and power change curves of the temperature difference sheet are shown in Fig. 11, Fig. 12 and Fig. 13.

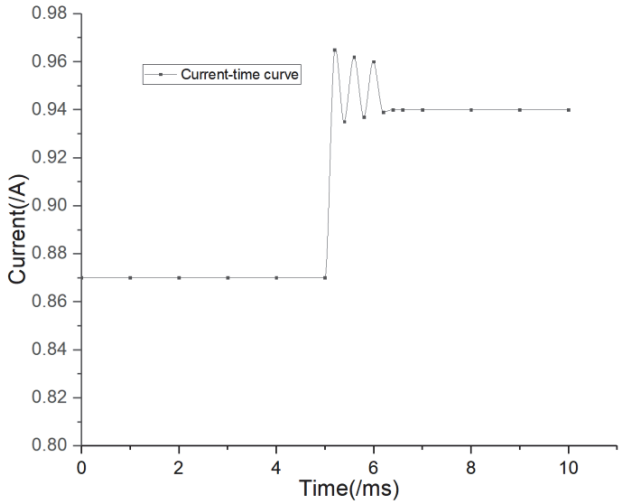


**Figure 11** Current time curve

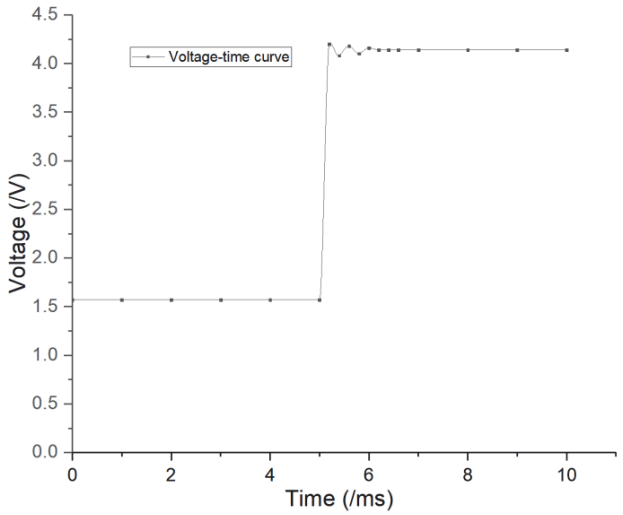


**Figure 12** Voltage time curve

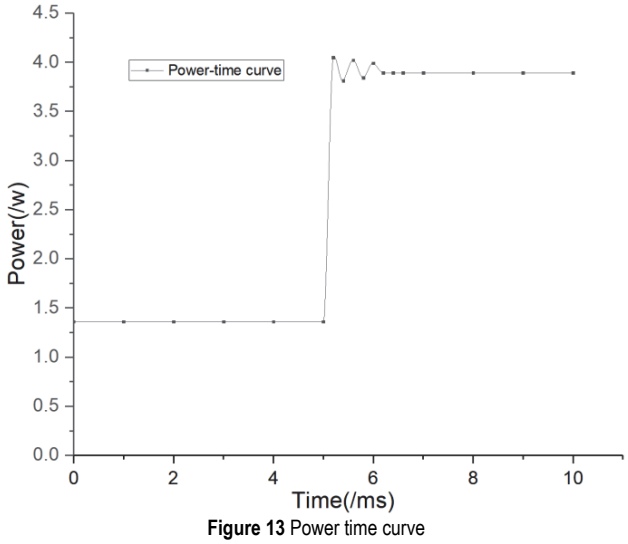


**Figure 13** Power time curve

At 5 ms, the temperature difference rapidly increases from 20 ℃ to 50 ℃. Under the action of MPPT, the current increases from 0.87 A to 0.94 A, the voltage increases from 1.57 V to 4.14 V, and the output power changes from 1.36 w to 3.89 w, which takes about 1.4 ms.

The supercapacitor group is 5.5 V/2 F. When the input conditions are the same, Fig. 14 shows the comparison of the charging curves of the supercapacitor group. Curve 1 shows the charging curve without power tracking, and curve 2 shows the charging curve with power tracking.

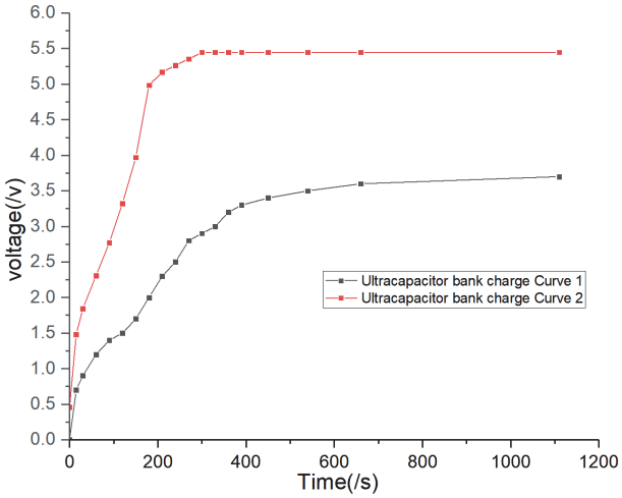


**Figure 14** Super capacitor bank charging curve

Based on the 3 V voltage point, the charging time of the ultracapacitor group with power tracking is about 120 s, and that without power tracking is about 330.

As can be seen from Fig. 11, Fig. 12, Fig. 13 and Fig. 14, maximum power tracking can be applied in thermoelectric effect, and the heat energy collection and storage time after adopting maximum power tracking is significantly shortened (the 3 V reference point is about 210 s).

Install the test device on the domestic water heater as shown in Fig. 15. The rated power of the electronic flame used in the test is 300mW (3 V × 0.1 A). After the water heater is opened, the output power of the temperature difference sheet on the device tends to be stable after 5.5 s. The temperature difference is about 55 ℃, the water flow rate is about 1 m/s, and the output power is 3.72 W (3.66 V × 1.01 A).

**Figure 15** Application test

Absolute value of relative error with test value $\Delta$ [31]:

$$\Delta = \left|\frac{3.72 - 3.98}{3.98}\right| \times 100\% = 6.5\% \quad (10)$$

$\Delta$ is less than 7%, indicating that the completed hot water energy collection device can be applied.

## 5 CONCLUSIONS

The optimized energy feedback controller of the disturbed gas water heater uses the pipeline structure design to enhance the turbulent velocity and the heat transfer coefficient, which improves the energy feedback utilization rate of the gas water heater pipeline. The method maintains high heat transfer efficiency and robustness. This research enables self-powered supply of gas water heaters to reduce the need for external power supply.

### Acknowledgement

Foundation Information: Humanities and Social Science Fund of Ministry of Education, China; 21XJA630004.

## 6 REFERENCES

[1] Fernando, X. & Lăzăroiu, G. (2023). Spectrum Sensing, Clustering Algorithms, and Energy-Harvesting Technology for Cognitive-Radio-Based Internet-of-Things Networks. *Sensors*, *23*(18), 7792. https://doi.org/10.3390/s23187792

[2] Wang, Y., Hong, M., Venezuela, J., Liu, T., & Dargusch, M. (2023). Expedient secondary functions of flexible piezoelectrics for biomedical energy harvesting. *Bioactive Materials*, *22*, 291-311. https://doi.org/10.1016/j.bioactmat.2022.10.003

[3] Wang, T. (2023). Pendulum-based vibration energy harvesting: Mechanisms, transducer integration, and applications. *Energy Conversion and Management*, *276*, 116469. https://doi.org/10.1016/j.enconman.2022.116469

[4] Gao, C., Liu, T., Luo, B., Cai, C., Zhang, W., Zhao, J., ... & Nie, S. (2023). Cellulosic triboelectric materials for stable energy harvesting from hot and humid conditions. *Nano Energy*, *111*, 108426. https://doi.org/10.1016/j.nanoen.2023.108426

[5] Dong, C., Shi, Y., Li, Q., Gu, H., Li, D., Ye, Y., & Li, T. (2023). An analysis on comprehensive influences of thermoelectric power generation based on waste heat recovery. *Thermal Engineering*, *44*, 102867. https://doi.org/10.1016/j.csite.2023.102867

[6] Lan, S., Li, Q., Guo, X., Wang, S., & Chen, R. (2023). Fuel saving potential analysis of bifunctional vehicular waste heat recovery system using thermoelectric generator and organic Rankine cycle. *Energy*, *263*, 125717. https://doi.org/10.1016/j.energy.2022.125717

[7] Lan, Y., Lu, J., Mu, L., Wang, S., & Zhai, H. (2023). Waste heat recovery from exhausted gas of a proton exchange membrane fuel cell to produce hydrogen using thermoelectric generator. *Applied Energy*, *334*, 120687. https://doi.org/10.1016/j.apenergy.2023.120687

[8] Chen, L., Ren, J., Gong, J., Qu, J., & Niu, R. (2023). Cost-effective, scalable fabrication of self-floating xerogel foam for simultaneous photothermal water evaporation and thermoelectric power generation. *Chemical Engineering Journal*, *454*, 140383. https://doi.org/10.1016/j.cej.2022.140383

[9] Ren, J., Chen, L., Gong, J., Qu, J., & Niu, R. (2023). Hofmeister effect mediated hydrogel evaporator for simultaneous solar evaporation and thermoelectric power generation. *Chemical Engineering Journal*, *458*, 141511. https://doi.org/10.1016/j.cej.2023.141511

[10] Ying, L., Huang, Z., Dong, Y., Lin, F., Ding, J., Wang, W., & Lu, J. (2023). Hybrid nanoarchitectonics of carbon/titanium carbide integrated hydrogel/melamine foam for highly efficient solar steam and thermoelectric power generation. *Desalination*, *549*, 116328. https://doi.org/10.1016/j.desal.2022.116328

[11] Avila, M., Barkley, D., & Hof, B. (2023). Transition to turbulence in pipe flow. *Annual Review of Fluid Mechanics*, *55*, 575-602. https://doi.org/10.1146/annurev-fluid-120720-025957

[12] Dubief, Y., Terrapon, V. E., & Hof, B. (2023). Elasto-inertial turbulence. *Annual Review of Fluid Mechanics*, *55*, 675-705. https://doi.org/10.1146/annurev-fluid-032822-025933

[13] Marino, R. & Sorriso-Valvo, L. (2023). Scaling laws for the energy transfer in space plasma turbulence. *Physics Reports*, *1006*, 1-144. https://doi.org/10.1016/j.physrep.2022.12.001

[14] Küchler, C., Bewley, G. P., & Bodenschatz, E. (2023). Universal velocity statistics in decaying turbulence. *Physical Review Letters*, *131*(2), 024001. https://doi.org/10.1103/PhysRevLett.131.024001

[15] Fan, Z. Guan, Y. (2021). Face Recognition Based on Full Convolutional Neural Network Based on Transfer Learning Model. *Computer Science and Information Systems*, *18*(4), 1395-1409. https://doi.org/10.2298/CSIS200922028F

[16] Katche, M. L., Makokha, A. B., Zachary, S. O., & Adaramola, M. S. (2023). A comprehensive review of maximum power point tracking (mppt) techniques used in solar pv systems. *Energies*, *16*(5), 2206. https://doi.org/10.3390/en16052206

[17] Zheng, S., Shahzad, M., Asif, H. M., Gao, J., & Muqeet, H. A. (2023). Advanced optimizer for maximum power point tracking of photovoltaic systems in smart grid: A roadmap towards clean energy technologies. *Renewable Energy*, *206*, 1326-1335. https://doi.org/10.1016/j.renene.2023.01.023

[18] Aygül, K., Cikan, M., Demirdelen, T., & Tumay, M. (2023). Butterfly optimization algorithm based maximum power point tracking of photovoltaic systems under partial shading condition. *Energy Sources, Part A: Recovery, Utilization, and Environmental Effects*, *45*(3), 8337-8355. https://doi.org/10.1080/15567036.2019.1677818

[19] Gen, M. & Lin, L. (2023). *Genetic algorithms and their applications*. Springer handbook of engineering statistics, London, Springer London. https://doi.org/10.1007/978-1-4471-7503-2_33

[20] Li, Q., Xu, J., Shu, L., Yan, F., Pang, B., & Peng, S. (2023). Exploration of the induced fluid-disturbance effect in CBM co-production in a superimposed pressure system. Energy, 265, 126347. https://doi.org/10.1016/j.energy.2022.126347

[21] Li, L., Tan, Y., Xu, W., Ni, Y., Yang, J., & Tan, D. (2023). Fluid-induced transport dynamics and vibration patterns of multiphase vortex in the critical transition states. *International Journal of Mechanical Sciences*, *252*, 108376. https://doi.org/10.1016/j.ijmecsci.2023.108376

[22] Weiyao, X., Ting, X., & Changqiang, J. (2021). Background Modeling from Video Sequences via Online Motion-Aware RPCA. Computer Science and Information Systems, 18(4), 1411-1426. https://doi.org/10.2298/CSIS200930029W

[23] Zhao, Y., Zhang, P., Lei, L., Kong, L., Galindo-Torres, S. A., & Li, S. Z. (2023). Metaball-Imaging discrete element lattice Boltzmann method for fluid-particle system of complex morphologies with case studies. *Physics of Fluids*, *35*(2). https://doi.org/10.1063/5.0135834

[24] Yin, L., Sun, M., Jiang, P., Dang, C., & Jia, L. (2023). Heat transfer coefficient and pressure drop of water flow boiling

in porous open micro channels heat sink. *Applied Thermal Engineering*, *218*, 119361. https://doi.org/10.1016/j.applthermaleng.2022.119361

[25] Li, H. & Hrnjak, P. (2023). A mechanistic model in annular flow in microchannel tube for predicting heat transfer coefficient and pressure gradient. *International Journal of Heat and Mass Transfer*, *203*, 123805. https://doi.org/10.1016/j.ijheatmasstransfer.2022.123805

[26] Katche, M. L., Makokha, A. B., Zachary, S. O., & Adaramola, M. S. (2023). A comprehensive review of maximum power point tracking (mppt) techniques used in solar pv systems. *Energies*, *16*(5), 2206. https://doi.org/10.3390/en16052206

[27] Sharma, A. K., Pachauri, R. K., Choudhury, S., Minai, A. F., Alotaibi, M. A., Malik, H., & Márquez, F. P. G. (2023). Role of metaheuristic approaches for implementation of integrated MPPT-PV systems: a comprehensive study. *Mathematics*, *11*(2), 269. https://doi.org/10.3390/math11020269

[28] Tan, W. H. & Mohamad-Saleh, J. (2023). Critical Review on Interrelationship of Electro-Devices in PV Solar Systems with Their Evolution and Future Prospects for MPPT Applications. *Energies*, *16*(2), 850. https://doi.org/10.3390/en16020850

[29] Ahmed, N., Sher, H. A., Al-Durra, A., & Hasanien, H. M. (2023). Comprehensive analysis and design of a switched-inductor type low inductance-requirement DC-DC buck-boost converter for low power applications. *IET Power Electronics*. https://doi.org/10.1049/pel2.12465

[30] Russo, A. & Cavallo, A. (2023). Stability and Control for Buck-Boost Converter for Aeronautic Power Management. *Energies*, *16*(2), 988. https://doi.org/10.3390/en16020988

[31] Cheklat, L., Amad, M., Omar, M., & Boukerram, A. (2021). Chearp: Chord-based Hierarchical Energy-Aware Routing Protocol for Wireless Sensor Networks. *Computer Science and Information Systems*, *18*(3), 813-834. https://doi.org/10.2298/CSIS200308043C

**Contact information:**

**Qian WANG**
(Corresponding author)
School of Electronic Information Engineering,
Geely University of China,
Chengdu, 641423
E-mail: wq_cduestc@163.com

**Wei LI**
School of Electronic Information Engineering,
Geely University of China,
Chengdu, 641423

**Xue-qin MENG**
School of Electronic Information Engineering,
Geely University of China,
Chengdu, 641423

**Chun-lan LI**
School of Electronic Information Engineering,
Geely University of China,
Chengdu, 641423